Mast Cells Are the Trigger of Small Vessel Disease and Diastolic Dysfunction in Diabetic Obese Mice

Sarah Guimbal, Lauriane Cornuault, Paul Rouault, Pierre-Louis Hollier, Candice Chapouly, Marie-Lise Bats, Julien Imbault, Alain-Pierre Gadeau, Thierry Couffinhal, Marie-Ange Renault

Title page

Mast cells are the trigger of small vessel disease and diastolic dysfunction in diabetic obese mice

Authors and affiliations

Sarah Guimbal, PhD[1], Lauriane Cornuault, MS[1], Paul Rouault, MS[1], Pierre-Louis Hollier, PhD[1], Candice Chapouly, PharmD, PhD[1], Marie-Lise Bats, PharmD, PhD[1], Julien Imbault, MD[1], Alain-Pierre Gadeau, PhD[1], Thierry Couffinhal, MD, PhD[1*] and Marie-Ange Renault, PhD[1*]

* These authors contributed equally to this work

[1] Univ. Bordeaux, Inserm, Biology of Cardiovascular Diseases, U1034, CHU de Bordeaux, F-33604 Pessac, France

Running title

Mast cells promote diastolic dysfunction

Corresponding author

Marie-Ange Renault

Inserm U1034

1, avenue de Magellan

33604 Pessac

France

e-mail : marie-ange.renault@inserm.fr

Tel : (33) 5 57 89 19 79

Keywords: Mast cells, endothelial dysfunction, diastolic dysfunction, cardiovascular risk factors.

Subject terms

Animal Models of Human Disease, Diabetes, Type 2, Heart Failure, Coronary Circulation, Endothelium/Vascular Type/Nitric Oxide

Abstract

Objective: Heart failure with preserved ejection fraction (HFpEF) is a major healthcare issue which has been difficult to manage to date, due to its complex and not well understood pathophysiology. Specifically, if a wealth of literature focuses on HFpEF cardiac component, very little information can be found on its vascular component. Our goal is to unravel the critical role of cardiac small vessel disease in the pathophysiology of diastolic dysfunction. **Approach and Results:** To do so, we used Leptin receptor deficient ($Lepr^{db/db}$) female mice, a recognized model of diastolic dysfunction. In these mice, the increased end diastolic pressure (EDP) signing diastolic dysfunction is associated with vascular leakage, endothelial cell activation and leucocyte infiltration. Strikingly, a RNA sequencing analysis of the cardiac vascular fraction of both $Lepr^{db/db}$ and control mice confirmed endothelial dysfunction and systemic inflammation, but above all, revealed a strong increase in several mast cell markers (notably FceR1a, Tryptase and Chymase). We then confirmed this accumulation of activated mast cells in the heart of $Lepr^{db/db}$ mice via histology. Importantly, we found that both mast cell degranulation inhibition and specific histamine blockade reduced vascular leakage, leucocyte infiltration and subsequently EDP in $Lepr^{db/db}$ mice. This demonstrated, for the first time, that mast cells, via histamine release, participate in the development of cardiac small vessel disease leading to diastolic dysfunction. **Conclusions:** Cardiac small vessel disease is a key mechanism of HFpEF pathophysiology that can be targeted to prevent the occurrence of diastolic dysfunction, by using both mast cell stabilizers and antihistaminic drugs.

Non standard abbreviations

HF	heart failure
EF	ejection fraction
HFpEF	heart failure with preserved ejection fraction
HFrEF	heart failure with reduced ejection fraction
LV	left ventricular
Vcam1	vascular cell adhesion molecule-1
Icam1	intercellular adhesion molecule-1
NOS3	nitric oxide synthase 3
Lepr	Leptin receptor
ESV	end-systolic volume
EDV	end-diastolic volume
LVPW	left ventricular posterior wall
IVS	inter-ventricular septum
LVID	left ventricular internal diameter
Cdh5	Cadherin-5
WGA	Wheat Germ Agglutinin
Ccl7	Chemokine (C-C motif) ligand 7
Il-6	Interleukin-6
Fcer1a	High affinity immunoglobulin epsilon receptor subunit alpha
H1R	Histamine H1 receptor
SMA	Alpha Smooth Muscle Actin
NO	nitric oxide

Introduction

A significant proportion of patients with clinical syndrome of heart failure (HF) happens to have a normal ventricular ejection fraction (EF) referred to as heart failure with preserved ejection fraction (HFpEF) as opposed to patients with reduced ejection fraction (HFrEF) [1]. HFpEF currently accounts for about 50% of all HF patients, and its prevalence relative to HFrEF is rising at a rate of approximately 1% per year. HFpEF patients are generally older, more often female and have a high prevalence of cardiovascular and non-cardiovascular comorbidities, such as obesity, metabolic syndrome, diabetes mellitus type 2, hypertension, atrial fibrillation or renal dysfunction [1]. HFpEF is diagnosed in the presence of HF signs and/or symptoms, preserved systolic left ventricular (LV) function, with an LV ejection fraction >50% and LV end-diastolic volume index <97 ml/m² with evidence of diastolic LV dysfunction [2]. In recent years, there have been significant advances in understanding aetiologies and mechanisms of HFrEF, leading to new therapeutic options. In contrast, if some progresses on HFpEF pathophysiology have been made, therapeutic targets are still missing and no therapies are available to reduce hospitalization or mortality for HFpEF patients. There is, therefore, an urgent need for a better understanding of HFpEF pathophysiology in order to develop new drugs [3]. A unifying, however untested**,** theory of the pathophysiology of HFpEF suggests that comorbidities lead to a systemic low grade inflammation, which triggers coronary microvascular dysfunction [2,4–6] and subsequently heart failure.

Endothelial dysfunction mostly refers to impaired endothelium-dependent, nitric oxide-mediated vasorelaxation. Nevertheless, endothelial dysfunction actually regroups an ensemble of features that includes acquirement of a pro-inflammatory /pro-thrombotic

phenotype due to an increased expression of adhesion and pro-thrombotic molecules such as vascular cell adhesion molecule-1 (Vcam1) and intercellular adhesion molecule-1 (Icam1), abnormal vascular leakage due to altered endothelial intercellular junctions and endothelial dedifferentiation promoting endothelial to mesenchymal transition [7]. EC dysfunction may then lead to a compromised heart perfusion because of impaired nitric oxide (NO)-dependent vasodilatation, cardiac oedema or thrombi formation. Besides, it may also promote cardiac fibrosis and inflammation [4,5,8]. Finally, an impaired production of endothelial-derived active substances as NO, endothelin-1, angiotensin II, Neuregulin is also proposed to directly affect cardiomyocyte passive tension[9–11].

What is known so far is that HFpEF is associated with an increased endothelial expression of ICAM-1 and E-selectin, an increased oxidative stress and a decreased nitric oxide synthase 3 (NOS3) activity both in animal models and in patients [12]. Also, brachial artery flow-mediated dilation assessment and laser Doppler flow measurement have revealed an impaired vascular and microvascular function in patients with HFpEF [5]. Finally, HFpEF is typically associated with increased myocardial stiffening (including increased cardiomyocyte passive stiffness and accumulation of stiff and resistant collagen fibres). Nevertheless the causal role of endothelial dysfunction in the pathophysiology of HFpEF has never been established.

In the present study we used Leptin receptor (Lepr)$^{db/db}$ female mice as a model of HFpEF to further characterize the phenotype and mechanisms of cardiac microvessel dysfunction associated with diastolic dysfunction. Notably, Lepr$^{db/db}$ female mice recapitulate the main risk factors for HFpEF i.e. obesity, diabetes and female sex. As a major breakthrough, this study demonstrates for the first time that abnormally increased mast cell activation

participates in the pathophysiology of both cardiac microvessel disease and diastolic dysfunction in Lepr$^{db/db}$ female mice.

Methods

The authors declare that all supporting data are available within the article and its online supplementary files.

Mice

Lepr^{db} mice (BKS.Cg-*Dock7*^{m}/+ *Lepr*^{db}/+J) were obtained from Charles River laboratories and bred together in our animal facility to obtain Lepr$^{db/db}$ and control Lepr^{db}/+ mice.

Animal experiments were performed in accordance with the guidelines from Directive 2010/63/EU of the European Parliament on the protection of animals used for scientific purposes and approved by the local Animal Care and Use Committee of Bordeaux University. Only females were used. Mice were either sacrificed by cervical dislocation or exsanguination under deep anesthesia (ketamine 100 mg/kg and xylazine 20 mg/kg, IP).

Cromolyn Sodium/Cetirizine therapy

To prevent mast cell degranulation, mice were treated with 50 mg/kg/day cromolyn sodium (Abcam) via intra-peritoneal injections for 28 days. Untreated mice received 0,9% NaCl daily intra-peritoneal injections. To investigate the role of Histamine release by mast cell, mice were treated with 4 mg/kg/day cetirizine (Arrow Génériques) orally (in the drinking water) for 28 days.

Echocardiography

Left-ventricular ejection fraction and LV dimension were measured on a high-resolution echocardiographic system equipped with a 30-MHz mechanical transducer (VEVO 2100, VisualSonics Inc.) as previously described [13,14]. Mice were anchored to a warming platform in a supine position, limbs were taped to the echocardiograph electrodes, and chests were shaved and cleaned with a chemical hair remover to minimize ultrasound attenuation. UNI'GEL ECG (Asept Inmed), from which all air bubbles had been expelled, was applied to the thorax to optimize the visibility of the cardiac chambers. Ejection fractions were evaluated by planimetry as recommended [15]. Two-dimensional, parasternal long-axis and short-axis views were acquired, and the endocardial area of each frame was calculated by tracing the endocardial limits in the long-axis view, then the minimal and maximal areas were used to determine the left-ventricular end-systolic (ESV) and end-diastolic (EDV) volumes, respectively. The system software uses a formula based on a cylindrical-hemiellipsoid model (volume=8.area²/3π/ length) [16]. The left-ventricular ejection fraction was derived from the following formula: (EDV- ESV)/EDV*100. The cardiac wall thickness, left ventricular posterior wall (LVPW), inter-ventricular septum (IVS) and left ventricular internal diameter (LVID) were calculated by tracing wall limits in both the long and short axis views.

LV pressure /systolic blood pressure measurement

LV diastolic pressure measurement was assessed via invasive catheterization technique. Briefly, mice were anesthetized with Isoflurane. A Scisense pressure catheter (Transonic) was inserted into the LV through the common carotid artery. Pressure was recorded using

LabChart software. End diastolic pressure, dP/dt minimum and maximum, Tau and heart rate were automatically calculated by a curve fit through end-systolic and end-diastolic points on the pressure plot.

Lung edema assessment

Lung edema was quantified using the wet/dry weight ratio. The wet weight was measured immediately after the lung was harvested, while the dry weight was measured after the lung was incubated for 72 hours at 85°C.

Immuno-histological assessments

Prior to staining, heart were stopped in diastole using KCl, perfused and then fixed with 10% formalin for 4 hours, paraffin embedded and cut into 7 µm thick sections. Alternatively, heart were fresh frozen in OCT, then cut into 7 µm thick sections.

ECs were identified using rat anti-CD31 antibodies (Histonova, cat# DIA-310) or FITC-labelled Isolectin B4 (Sigma Aldrich, Cat#L2895). Smooth muscle cells were identified using Cy3-conjugated mouse anti- Alpha Smooth Muscle Actin (SMA) antibodies (Sigma Aldrich, Cat#C6198). Albumin was stained using sheep anti-albumin antibodies (Abcam, Cat# ab8940). Pan-leucocytes were identified using rat anti-mouse CD45 antibodies (BD Pharmingen Inc, Cat# 550539). Macrophages were identified using rat anti-CD68 antibodies (Biolegend, Cat# 137001). M2 macrophages were identified using goat anti-mannose Receptor C-Type 1 (Mrc1) antibodies (R&D systems, Cat# AF1556). Neutrophils were identified using rat anti-Ly6G antibodies (BD Pharmingen Inc, Cat# 551459). T lymphocytes were identified using goat anti-CD3 antibodies (Santa Cruz Biotechnology, Inc, Cat# sc-1127). B-cells were stained using rat anti-B220/CD45R antibodies (R&D systems, Cat# MAB1217)

Mast/Stem Cell Growth Factor Receptor c-Kit was identified using goat anti-CD117 antibodies (R&D systems, Cat# AF1356). Fcer1a was identified using rabbit anti-Fcer1a antibodies (Biorbyt, Cat# orb41809). Cardiomyocytes were immunostained using rabbit anti-desmin antibodies (DB 148, Cat#DB148), mouse anti-sarcomeric actin antibodies (Sigma, Cat# A2172) and rabbit anti-connexin-43 (Cx43) antibodies (Sigma, Cat# C6219). Endothelial adherens junction integrity was assessed using mouse anti-Cadherin-5 (Cdh5) antibodies (Santa Cruz Biotechnology, Inc, Cat# sc-9989).

For immunofluorescence analyzes, primary antibodies were resolved with Alexa Fluor®–conjugated secondary polyclonal antibodies (Invitrogen, Cat# A-21206, A-21208, A-11077, A-11057, A-31573, A-10037) and nuclei were counterstained with DAPI (1/5000). Negative controls using secondary antibodies only were done to check for antibody specificity.

Cardiomyocyte membranes were stained using Wheat Germ Agglutinin (WGA), Alexa Fluor™ 488 Conjugate (Invitrogen).

Fibrosis was quantified after Sirius red staining of heart sections by quantifying the percentage of red-positive area. Cardiomyocyte mean surface area was measured using the Image J software after membrane staining with Wheat Germ Agglutinin (WGA), Alexa Fluor™ 488 Conjugate (Invitrogen) in 5 pictures randomly taken under x630 magnification. Pictures were taken in areas where cardiomyocytes were oriented transversally. Capillary density (CD31+ vessels) was quantified in 4 pictures taken under x260 magnification in areas where cardiomyocytes were oriented transversally.

To assess the mean capillary diameter, the diameter of 10 capillaries randomly chosen in each picture was measured via Image J. Inflammatory cell density (CD45+, CD68+, CD3+ and Ly6G+) was quantified in 8 pictures randomly taken under x260 magnification. Mast cell

density and mast cell degranulation was assessed after Toluidine blue staining of heart sections. Mast cells were counted in the entire section.

All pictures and quantifications (done using ImageJ/Fiji v2.0.0-rc-59 software (National Institute of Health, USA)) were performed by a blinded investigator. More precisely, all samples were assigned a random number prior to animal sacrifice, data collection and analysis. At the end of the experiment, the genotype/treatment for each animal was unveiled to allow data comparison and experimental conclusion.

Measurement of Reactive Oxygen Species (ROS)

Fresh frozen heart sections were incubated with 1 µmol/L dihydroethidium (Sigma Aldrich, Cat# 37291**)** for 10 minutes at room temperature. Red fluorescence was quantified in 8 pictures randomly taken under x400 magnification using Image J software.

Quantitative RT-PCR

RNA was isolated using Tri Reagent® (Molecular Research Center Inc) as instructed by the manufacturer, from heart tissue that had been snap-frozen in liquid nitrogen and homogenized. For quantitative RT-PCR analyses, total RNA was reverse transcribed with M-MLV reverse transcriptase (Promega) and amplification was performed on an AriaMx Real Time PCR system (Agilent Technologies) using B-R SYBER® Green SuperMix (Quanta Biosciences). Primer sequences are reported in Supplementary table 1.

The relative expression of each mRNA was calculated by the comparative threshold cycle method and normalized to 18S rRNA expression.

Soluble/insoluble collagen measurement

Total cardiac collagen and insoluble cardiac collagen were quantified using the Sircol™ Soluble Collagen Assay and The Sircol™ INSOLUBLE Collagen Assay (Biocolor) according to the manufacturer's instructions.

Western blot analysis

Plamatic IgE level was evaluated by SDS PAGE using rat anti-mouse IgE antibodies (R&D systems Cat# MAB9935). Nos3 and phosphorylated Nos3 levels were evaluated by SDS PAGE using rabbit anti-Nos3 (Cell signaling technology, Cat#32027) and rabbit anti phospho-Nos3 (S1177) (Cell signaling technology, Cat#9571) antibodies respectively. Icam1, Vcam1, Chemokine (C-C motif) ligand 7 (Ccl7) and Interleukin-6 (Il-6) protein levels were evaluated by SDS PAGE using goat anti-Icam-1 (R&D systems Cat# AF-796), rabbit anti-Vcam-1 (abcam, Cat# ab134047), goat anti-Ccl7 (R&D systems Cat# AF-456) and goat anti-Il-6 (R&D systems Cat# AF-406) antibodies respectively. Protein loading quantity was controlled using mouse monoclonal anti-a-tubulin antibodies (Sigma, Cat# T5168).

Statistics

Results are reported as mean ± SEM. Comparisons between groups were analyzed for significance with the non-parametric Mann-Whitney test, the Kruskal-Wallis test followed by Dunn's multiple comparison test (for more than two groups) or a 2 way ANOVA followed by Sidak's multiple comparison test (for kinetics analyses) using GraphPad Prism v8.0.2 (GraphPad Inc, San Diego, Calif). The normality and variance were not tested. Differences between groups were considered significant when $p \leq 0.05$ (*: $p \leq 0.05$; **: $p \leq 0.01$; ***: $p \leq 0.001$).

Results

Lepr$^{db/db}$ female mice have diastolic dysfunction from 3 months of age.

First we quantified and characterized the kinetics of appearance of cardiovascular risk factors in the Lepr$^{db/db}$ female mice and in their control Lepr^{db}/+ littermates bred in our laboratory. Lepr$^{db/db}$ female mice are significantly overweight from 6 weeks of age while diabetes appears from 3 months of age. Plasmatic HDL cholesterol is elevated from 6 weeks of age while LDL cholesterol is only increased after 6 months of age. Plasmatic triglycerides are elevated from 3 months of age. Besides Lepr$^{db/db}$ female mice have mild hypertension from 3 months of age and display significantly increased circulating leucocytes (monocytes and neutrophils) later in life at 1 year of age (Supplemental Figure I).

Then we assessed cardiac function in these mice mainly via echocardiography and LV catheterization. Lepr$^{db/db}$ female mice have normal ejection fraction (≥50%) during at least their first year of life (Figure 1A). However, they display diastolic dysfunction attested by a significantly increased end diastolic pressure (EDP) from 3 months of age (Figure 1B) and an increased lung water content signing pulmonary edema (Figure 1C). However, the maximum and minimum dP/dt, the relaxation time constant Tau and the heart rate were not modified at rest (Supplemental Figure II A-D). Increased EDP was associated with increased heart weight/tibia length ratio and increased diastolic LV posterior wall thickness attesting cardiac hypertrophy (Figure 1D-E). Diastolic LV internal diameter was not different from that of control mice (Figure 1F). Consistent with cardiac hypertrophy, cardiomyocyte were significantly larger in 3 month old Lepr$^{db/db}$ female mice compared to control mice (Figure 1G, H). Myocyte dedifferentiation, attested by myosin heavy chain 7 (Myh7) over expression appears later on at 6 months of age (Figure 1I). Notably, while both cardiac atrial natriuretic

peptide (ANP) and brain natriuretic peptide (BNP) mRNA expression increased with age, they were not different in Lepr$^{db/db}$ mice and control mice (Supplemental Figure II E-F).

Altogether, this first set of data confirmed that Lepr$^{db/db}$ mice have diastolic dysfunction with preserved systolic function and may be used as a mouse model of HFpEF. Notably this is consistent with previous investigations [17,18].

Lepr$^{db/db}$ female mice do not have cardiomyocyte gross anomalies.

To search for cardiomyocyte major anomalies, we first performed Desmin and sarcomeric alpha actin staining on heart cross sections to visualize cardiomyocyte sarcomeres and Cx43 staining to identify intercalary disks. We did not observe any significant difference between Lepr$^{db/db}$ mice and their control littermates (Supplemental Figure IIIA-B). Then we performed RT-qPCR to measure expression level of several cardiomyocyte markers notably, Titin isoforms N2-A and N2-B, Myocyte-specific enhancer factor 2C (MEF2C), Cx43, Sarcoplasmic/endoplasmic reticulum calcium ATPase 2 (Serca2) and Cardiac phospholamban (Pln) (Supplemental Figure IIIC-H). None of these markers were significantly different in Lepr$^{db/db}$ mice compared to their control littermates.

In conclusion, Lepr$^{db/db}$ female mice do not have cardiomyocyte gross anomalies, which is consistent with the unchanged dP/dT minimum and maximum.

Lepr$^{db/db}$ female mice do not have significant cardiac fibrosis.

Cardiac fibrosis, often associated with HFpEF, was first evaluated via picroSirius red staining. As shown in supplemental figure III, the red staining was equivalent in 3 month old Lepr$^{db/db}$

and in their control littermates (Supplemental Figure IVA-B). This result was confirmed using the Sircol™ collagen assay (Supplemental Figure IVC). Moreover collagen type I alpha 1 chain (Col1a1) mRNA expression was not modified, while collagen type III alpha 1 chain (Col3a1) mRNA expression was diminished (Supplemental Figure IV-E). Finally, no difference in Lysyl oxidase (Lox) mRNA expression, an enzyme promoting collagen cross linking was observed (Supplemental Figure IVF). To test whether cardiac fibrosis may appear later in life, we performed the same assays in a year old animals. Similarly to what we found in 3 month old animal, neither picrosirius red stain nor the Sircol™ collagen assay showed any differences between $Lepr^{db/db}$ mice and control littermates (Supplemental Figure IVG-H). Although Lox mRNA was significantly increased in a year old $Lepr^{db/db}$ mice compared to their control littermates (Supplemental Figure IVJ), it did not lead to increased amount of insoluble collagen in the heart (Supplemental Figure IVK).

In conclusion, diastolic dysfunction in $Lepr^{db/db}$ female mice is not associated with increased cardiac fibrosis.

3 month old $Lepr^{db/db}$ female mice have cardiac microvessel disease.

To phenotype the cardiac microvessel of 3 month old $Lepr^{db/db}$ female mice, we performed both immuno-histological and gene expression analyses. Gene expression analysis was performed by a transcriptomic analysis via RNA sequencing of the cardiac vascular fraction which includes ECs, pericytes, few smooth muscle cells and perivascular inflammatory cells (Supplemental Table II). The main RNA sequencing results were confirmed by RT-qPCR performed on total heart RNA samples.

First we quantified cardiac capillary density and found that capillary density is significantly decreased in the heart of Lepr$^{db/db}$ female mice (Figure 2A-B) which is fully consistent with previous analyses performed on human patients with HFpEF [19]. Besides, we found that the mean capillary diameter was significantly increased (Figure 2C) (notably cardiac capillaries are not muscularized), while the diameter of SMA+ arterioles was slightly but not significantly decreased (Figure 2D-E). Accordingly, transcriptomic analysis via RNA sequencing of the cardiac vascular fraction of these mice showed a switch in the balance between vasodilator and vasoconstrictor molecules in favor of vasoconstriction of cardiac arterioles (Figure 2F) notably, because of the downregulated expression of Apelin (Apln) and the increased expression of Type-1 angiotensin II receptor (Agtr1), Thromboxane-A synthase (Tbxas1), Arachidonate 5-lipoxygenase (Alox5) and Prostaglandin G/H synthase 2 (Ptgs2) (Figure 2F). However, Nos3 and phospho-Nos3 levels were not different in Lepr$^{db/db}$ and control mice (Figure 2G-I).

To assess vascular permeability we measure albumin extravasation and found a significantly increased albumin extravasation in Lepr$^{db/db}$ mice compared to their control littermates which indicate abnormal vessel permeability (Figure 2J-K). Besides, both the transcriptomic analysis and gene expression analysis showed a significant upregulation of multiple inflammatory cytokines including Il-6, chemokine (C-C motif) ligand 2 (Ccl2), chemokine C-C motif 3 ligand (Ccl3) and Ccl7 (Figure 3A-D). Il-6 and Ccl7 overexpression were confirmed at protein level (Figure 3D-F). Also, we found an increased mRNA expression of adhesion molecule Icam1 and E-selectin (Supplemental Figure VC-F). However, the increased Icam1 expression was not confirmed at protein level (Supplemental Figure VG-I). The transcriptomic analysis also revealed a pro-coagulation phenotype attested by P2Y purinoceptor 12 (P2ry12), Coagulation factor XIII A chain (F13a1) and Platelet factor 4 (PF4)

upregulation (Supplemental Figure VJ). Finally, we assessed oxidative stress which was not different in Lepr$^{db/db}$ and control mice via DHE staining (Supplemental Figure VA-B).

Altogether, these results demonstrate that Lepr$^{db/db}$ have cardiac microvessel disease characterized by a decreased capillary density but an increased capillary diameter. Moreover, they display a pro-inflammatory and a pro-coagulant phenotype.

3 month old Lepr$^{db/db}$ female mice have cardiac inflammation.

In association with upregulation of multiple inflammatory cytokines, leucocyte infiltration in the cardiac tissue of Ler$^{db/db}$ mice was significantly increased (Figure 3G-H). Among Leucocytes, cells were mostly CD68+/Mrc1+ M2 macrophages (Supplemental Figure VIA-B). Besides, leucocytes also included CD3+ T-lymphocytes (Supplemental Figure VIC-D), Ly6G+ neutrophils (Supplemental Figure VIE-F) and B220 B-lymphocytes (Supplemental Figure VIG-H). Both M2 macrophage and B-lymphocyte densities were increased in Lepr$^{db/db}$ mice. However, T-lymphocytes and neutrophils densities were not different between Lepr$^{db/db}$ mice and their control littermates.

3 month old Lepr$^{db/db}$ female mice have abnormal cardiac mast cell activation.

Apart from highlighting EC dysfunction and cardiac inflammation, transcriptomic analysis of the cardiac vascular fraction also revealed that among the 50 genes with log2FC≥2, 7 genes were mast cell markers (Figure 4A-B). We confirmed Carboxypeptidase A3, mast cell (Cpa3) and High affinity immunoglobulin epsilon receptor subunit alpha (Fcer1a) overexpression in total heart extracts via RT-qPCR (Figure 4C-D) and confirmed that Fcer1a was indeed expressed by CD45+, CD117+ cardiac mast cell (Figure 4E). We then quantified the total

number of cardiac mast cell after Toluidine blue staining of heart section. We found no significant differences between Lepr$^{db/db}$ mice and their control littermates (Figure 4F-G). However, when we calculated the percentage of activated/degranulating mast cells, we found that it was significantly increased in the heart of Lepr$^{db/db}$ mice (Figure 5A-B). Since mast cells are typically activated by IgE, we measured IgE circulating levels in plasma from Lepr$^{db/db}$ mice and control littermates. Consistent with increased mast cell activation, IgE circulating level were significantly increased in Lepr$^{db/db}$ mice (Figure 5C-D). However, the percentage of IgE positive, mast cells (Fcer1a+ cells) infiltrated in the heart of Lepr$^{db/db}$ mice was not increased compared to that of control mice (Figure 5E) suggesting that mast cells may be activated by another pathway. Alternatively, mast cells can be activated by the complement cascade of, which we found 9 genes to be significantly increased in the transcriptomic analysis (Figure 5F).

Mast cells are known to induce cardiovascular effects through the release of their granule content [20], notably proteases, histamine and the production of eicosanoids and cytokines. Consistent with increased cardiac mast cell activation, both Tryptase (Tpsab1) and Chymase (Cma1) mRNA were significantly increased in the heart of Lepr$^{db/db}$ mice compared to the one of their control littermates (Figure 5G-H). Also the transcriptomic analysis of the cardiac vascular fraction revealed increased eicosanoid metabolic process attested by increased arachidonate 5-lipoxygenase (Alox5), thromboxane A synthase 1 (Tbxas1) and leukotriene C4 synthase (Ltc4s) expression (Figure 5I). The increased Alox5 mRNA expression was confirmed in total heart samples via RT-qPCR (Figure 5J).

Activated cardiac mast cells, via histamine release, induce cardiac small vessel disease in Lepr$^{db/db}$ mice.

To investigate the role of mast cell degranulation in the pathophysiology of cardiac microvessel disease, we first performed *in vitro* assays using cultured ECs. More specifically, HUVECs were co-cultured in the presence of mast cells treated with plasma from $Lepr^{db/db}$ or control mice. We found that HUVEC permeability was significantly increased in the presence of mast cells activated with $Lepr^{db/db}$ plasma compared to mast cells treated with control plasma (Supplemental Figure VIIA). Notably, the plasma of $Lepr^{db/db}$ mice alone was not sufficient to increase HUVEC permeability (Supplemental Figure VIIB). Since mast cells are known to promote endothelium permeability through histamine release [21] via activation of H1R receptors, we evaluated endothelial adherens junction integrity in the presence or not for cetirizine, an H1R inhibitor. We found that mast cells treated with $Lepr^{db/db}$ plasma increased Cdh5 junction thickness in the absence of cetirizine but not in the presence of cetirizine (Supplemental Figure VIIC-D), demonstrating that mast cells treated with $Lepr^{db/db}$ plasma disrupt endothelial adherens junction via histamine release, notably, we also verified that histamine alone was sufficient to alter Cdh5 junctions integrity (Supplemental Figure VIIE-F).

To assess the role of mast cell activation *in vivo* in the heart, we first used cromolyn sodium, a mast stabilizer which inhibits mast cell degranulation. 2 month old $Lepr^{db/db}$ mice (i.e. before they display increased EDP) were treated with 50 mg/Kg/day cromolyn sodium versus vehicle. Mice were sacrificed 28 days later. We verified cromolyn sodium therapy was effective and did decrease the percentage of degranulating mast cells in the heart (Supplemental Figure VIIIA). Then, we investigated the effect of cromolyn sodium therapy on cardiac microvessel phenotype and cardiac inflammation. Cromolyn sodium therapy did not modify cardiac microvessel density (Supplemental Figure VIIIB), however it did reduce capillary diameter (Figure 6A-B) and permeability attested by decreased albumin

extravasation (Figure 6C-D). Moreover, CD45+ leucocyte, especially CD68+ macrophage, recruitment was significantly decreased (Figure 6E-F, Supplemental Figure VIIIC-F).

To summarize, mast cells promote cardiac capillary permeability and vasodilation, which is consistent with the well-known effect of histamine contained in mast cell granules [22]. To verify cardiac capillary permeability and vasodilation was indeed due to histamine, 2 month old $Lepr^{db/db}$ mice were treated with 4 mg/kg/day cetirizine versus vehicle. As expected, both the diameter of cardiac capillaries (Figure 6G-H) and their permeability (Figure 6I-IJ) were significantly reduced in $Lepr^{db/db}$ mice treated with cetirizine vs vehicle-treated $Lepr^{db/db}$ mice. Also, similarly, to cromolyn sodium therapy, cetirizine therapy significantly prevented CD68+ macrophage recruitment (Figure 6K-L, Supplemental Figure VIIIG-J).

In conclusion, mast cells promote cardiac small vessel disease via histamine release in $Lepr^{db/db}$ mice. Notably, cetirizine is a selective Histamine H1-receptor antagonist demonstrating that Histamine promotes cardiac capillary dilatation and leakage via Histamine H1-receptor.

Activated cardiac mast cells promote the appearance of diastolic dysfunction in $Lepr^{db/db}$ mice.

Finally, to measure the pathophysiological consequences of histamine-induced small vessel disease on cardiac function, we investigated cardiac function in both cromolyn sodium-treated and cetirizine-treated $Lepr^{db/db}$ mice. Ejection fraction, which is normal in $Lepr^{db/db}$ mice was modulated neither by cromolyn sodium treatment (Figure 7A) nor by cetirizine treatment (Figure 7B). However, EDP was significantly decreased in both cromolyn sodium-treated (Figure 7C) and cetirizine-treated (Figure 7D) $Lepr^{db/db}$ mice indicating improved

diastolic function. Neither Cromolyn sodium nor Cetirizine therapy did modify heart weight, LV posterior wall thickness or the mean cardiomyocyte size (Figure 7E-K), indicating that cromolyn sodium nor cetirizine therapy prevents cardiac hypertrophy.

Altogether these results indicated that mast cells, via secretion of their granule content, promote the development of diastolic dysfunction, however, they do not participate in the development of cardiomyocyte hypertrophy.

Discussion

The present study supports the microvascular hypothesis of HFpEF especially in the setting of obesity and type 2 diabetes. In this paper, we used $Lepr^{db/db}$ female mice as a model of diastolic dysfunction. $Lepr^{db/db}$ female mice have the advantage of recapitulating the main risk factors for HFpEF, i.e. diabetes, obesity female sex and hypertension. $Lepr^{db/db}$ mice were previously shown to display diastolic dysfunction [17,23,24] and to recapitulate significant features of human HFpEF [18,25]. In the present study, we thoroughly characterized the cardiac microvascular phenotype of these mice, notably, via a transcriptomic analysis. We revealed that cardiac microvessel disease is characterized by a decreased capillary density, abnormal vessel permeability and slight constriction of arterioles but increased capillary diameter; moreover we showed that ECs display oxidative stress and have a pro-inflammatory and pro-coagulant phenotype. Strikingly, we demonstrated for the first time that, in $Lepr^{db/db}$ mice, cardiac microvessel disease is associated with increased mast cell activation and proved that it participates to the pathophysiology of both cardiac microvessel disease and diastolic dysfunction (Supplemental Figure IX). More specifically, activated mast cells release histamine which increases capillary permeability and diameter via H1 receptors known to be expressed by endothelial cells.

The current paradigm for HFpEF proposes that myocardial remodelling and dysfunction in HFpEF results from the following sequence of events: 1) comorbidities including obesity, diabetes and/or hypertension would induce a systemic low grade pro-inflammatory state; 2) this pro-inflammatory state would induce EC dysfunction characterized by an increased ROS production, a decreased NO synthesis and an increased expression of adhesion molecules such as Vcam1 and E-selectin; 3) EC dysfunction would lead to a compromised heart perfusion secondary to impaired NO-dependent vasodilatation, oedema and pro-inflammatory/pro-thrombotic phenotype, macrophage infiltration and fibrosis [4,5]. The present data show that the $Lepr^{db/db}$ female mice model largely recapitulates this paradigm while adding further features. Notably, we demonstrated that mast cell activation, which is either part of the low grade pro-inflammatory state or induced by the low grade inflammatory state of diabetic obese mice, promotes microvascular dysfunction especially vascular permeability and capillary dilation and participates in the development of diastolic dysfunction. Consistent with a central role of inflammation [26] and microvascular disease in the pathophysiology of HFpEF, $Lepr^{db/db}$ mice do not display significant cardiac fibrosis or major cardiomyocyte abnormalities. Notably, we found that cardiomyocyte hypertrophy does not seem to promote the increased EDP. Indeed, although cromolyn sodium therapy prevents increased EDP, this effect is not associated to cardiomyocyte hypertrophy and dedifferentiation. Notably, increased EDP seen in HFpEF is not always due to cardiac hypertrophy since 31% of patients with HFpEF do not have cardiac hyperthrophy [27]. Besides cardiac hypertrophy is notably triggered by Nuclear factor of activated T-cells (NFAT) activation, NFAT is positively regulated by calmodulin/calcineurin but negatively regulated by Glycogen Synthase Kinase 3 Beta (GSK3β) [28]. So cardiac hypertrophy is likely secondary to insulin resistance in type 2 diabetic mice. The present paper highlight a causal role of mast

cell activation in obesity/diabetes-related increase in ventricular diastolic pressure since EDP is significantly decreased in both cromolyn and cetirizine treated mice. Considering that cromolyn and cetirizine treatment did not prevent cardiomyocyte hypertrophy, the present study suggests that the increased EDP in Lepr$^{db/db}$ mice is not due to cardiomyocyte hypertrophy while it might be secondary to endothelial dysfunction as suggested by Paulus et al paradigm [6]. The mechanism responsible for increased EDP remains to be identified.

Mast cells are immune cells that reside in the connective tissues including the myocardium. They are characterized by the expression of c-Kit receptors and by their granules containing active mediators including proteases, notably Cma1, Tpsab1 and histamine. Mast cells may be activated by IgEs via their receptor Fcer1a, Complement factors via Toll-like receptors, IgGs or cytokines [29]. They have been associated with several cardiovascular diseases including atherosclerosis, myocardial infarction and aneurysms [20], pathologies in which mast cells are contributing to the pathogenesis essentially through the release of their granule content. Importantly, circulating Tryptase was recently suggested to be a marker for cardiovascular diseases [30]. Moreover, mast cells have been previously involved in diastolic dysfunction induced by ovariectomy in rats [31] and diabetic cardiomyopathy in streptozotocin-treated mice [32]. The present study thus confirms the significant role of mast cells in cardiovascular diseases especially heart failure. How mast cells are activated in the setting of cardiovascular diseases remains unknown [29]. We found that, in Lepr$^{db/db}$ mice, increased activation of mast cells is associated with increased circulating levels of IgEs nevertheless; the amount of IgE bound cardiac to mast cells was not changed. IgE/Fcer1a is the main route of mast cell activation in allergic diseases. Interestingly, IgEs were reported to be elevated in the serum of patients with cardiovascular diseases [33] [34] [35] including coronary arterial disease and myocardial infarction. Consistently, asthma was shown to be

related to an increased incidence of coronary heart disease, particularly in women [36]. More specifically, one study reported that coronary flow reserve, considered as an early marker of endothelial dysfunction is significantly lower in patients with high IgE levels [37]. Altogether, these results further support that $Lepr^{db/db}$ mice are a relevant model of human cardiovascular diseases.

In conclusion, the present study further confirms that inflammation and cardiac microvessel disease are at the heart of HFpEF pathophysiology [26] and identified for the first time mast cells as critical players of cardiac microvessel disease and diastolic dysfunction, making them a promising therapeutic target for HFpEF treatment. Indeed the present study suggests that mast cell stabilizers are H1 receptor antagonists may be used to prevent the occurrence of heart failure. Notably, while H2 receptor antagonist are widely suggested to have beneficial effects in heart failure especially because of their negative inotropic and chronotropic effects [38]. The cardiac effects of H1 receptor antagonists remain poorly investigated. Interestingly, one study reported that H1 receptor antagonists may improve cardiac remodeling in patients on chronic hemodialysis [39]. Another study performed in mice reported that cetirizine improves cardiac remodeling associated with viral myocarditis [40].

Acknowledgments

We thank Philippe Alzieu, Annabel Reynaud, Sylvie Jeanningros, Sylvain Grolleau, and Maxime David for their technical help. We thank Christelle Boullé for administrative assistance.

This work benefited from equipment and services from the iGenSeq (RNA sequencing) and iCONICS (RNAseq analysis) core facilities at the ICM (Institut du Cerveau et de la Moelle épinière, Hôpital Pitié-Salpêtrière, PARIS, France).

Sources of Funding

This study was supported by grants from the Fondation pour la Recherche Médicale (équipe FRM), from the Region « Nouvelle Aquitaine » and the Agence Nationale pour la Recherche (Appel à Projet Générique). Finally, this study was co-funded by the "Institut National de la Santé et de la Recherche Médicale" and by the University of Bordeaux.

Disclosures

None declared

References

1. Pfeffer MA, Shah AM, Borlaug BA. Heart Failure With Preserved Ejection Fraction In Perspective. *Circ Res*. 2019;124(11):1598-1617. doi:10.1161/CIRCRESAHA.119.313572

2. Sharma K, Kass DA. Heart failure with preserved ejection fraction: mechanisms, clinical features, and therapies. *Circ Res*. 2014;115(1):79-96. doi:10.1161/CIRCRESAHA.115.302922 CIRCRESAHA.115.302922 [pii]

3. Lyle MA, Brozovich FV. HFpEF, a Disease of the Vasculature: A Closer Look at the Other Half. *Mayo Clin Proc*. 2018;93(9):1305-1314. doi:10.1016/j.mayocp.2018.05.001

4. Marti CN, Gheorghiade M, Kalogeropoulos AP, Georgiopoulou VV, Quyyumi AA, Butler J. Endothelial dysfunction, arterial stiffness, and heart failure. *J Am Coll Cardiol*. 2012;60(16):1455-1469. doi:S0735-1097(12)02523-5 [pii] 10.1016/j.jacc.2011.11.082

5. Marechaux S, Samson R, van Belle E, Breyne J, de Monte J, Dedrie C, Chebai N, Menet A, Banfi C, Bouabdallaoui N, Le Jemtel TH, Ennezat PV. Vascular and Microvascular Endothelial Function in Heart Failure With Preserved Ejection Fraction. *Journal of cardiac failure*. 2016;22(1):3-11.

6. Paulus WJ, Tschope C. A novel paradigm for heart failure with preserved ejection fraction: comorbidities drive myocardial dysfunction and remodeling through coronary microvascular endothelial inflammation. *J Am Coll Cardiol*. 2013;62(4):263-271. doi:S0735-1097(13)01890-1 [pii] 10.1016/j.jacc.2013.02.092

7. Li Y, Lui KO, Zhou B. Reassessing endothelial-to-mesenchymal transition in cardiovascular diseases. *Nat Rev Cardiol*. 2018;15(8):445-456. doi:10.1038/s41569-018-0023-y

8. D'Amario D, Migliaro S, Borovac JA, Restivo A, Vergallo R, Galli M, Leone AM, Montone RA, Niccoli G, Aspromonte N, Crea F. Microvascular Dysfunction in Heart Failure With Preserved Ejection Fraction. *Front Physiol*. 2019;10:1347. doi:10.3389/fphys.2019.01347

9. Tirziu D, Giordano FJ, Simons M. Cell communications in the heart. *Circulation*. 2010;122(9):928-937. doi:122/9/928 [pii] 10.1161/CIRCULATIONAHA.108.847731

10. Noireaud J, Andriantsitohaina R. Recent insights in the paracrine modulation of cardiomyocyte contractility by cardiac endothelial cells. *Biomed Res Int*. 2014;2014:923805. doi:10.1155/2014/923805

11. Schiattarella GG, Altamirano F, Tong D, French KM, Villalobos E, Kim SY, Luo X, Jiang N, May HI, Wang ZV, Hill TM, Mammen PPA, Huang J, Lee DI, Hahn VS, Sharma K, Kass DA, Lavandero S, Gillette TG, Hill JA. Nitrosative stress drives heart failure with preserved ejection fraction. *Nature*. 2019;568(7752):351-356. doi:10.1038/s41586-019-1100-z

12. Franssen C, Chen S, Unger A, Korkmaz HI, De Keulenaer GW, Tschope C, Leite-Moreira AF, Musters R, Niessen HW, Linke WA, Paulus WJ, Hamdani N. Myocardial Microvascular Inflammatory Endothelial Activation in Heart Failure With Preserved Ejection Fraction. *Jacc*. 2016;4(4):312-324.

13. Renault MA, Roncalli J, Tongers J, Misener S, Thorne T, Jujo K, Ito A, Clarke T, Fung C, Millay M, Kamide C, Scarpelli A, Klyachko E, Losordo DW. The Hedgehog transcription factor Gli3 modulates angiogenesis. *Circ Res*. 2009;105(8):818-826.

14. Roncalli J, Renault MA, Tongers J, Misener S, Thorne T, Kamide C, Jujo K, Tanaka T, Ii M, Klyachko E, Losordo DW. Sonic hedgehog-induced functional recovery after myocardial infarction is enhanced by AMD3100-mediated progenitor-cell mobilization. *J Am Coll Cardiol*. 2011;57(24):2444-2452.

15. Schiller NB, Shah PM, Crawford M, DeMaria A, Devereux R, Feigenbaum H, Gutgesell H, Reichek N, Sahn D, Schnittger I. Recommendations for quantitation of the left ventricle by two-dimensional echocardiography. American Society of Echocardiography Committee on Standards, Subcommittee on Quantitation of Two-Dimensional Echocardiograms. *J Am Soc Echocardiogr*. 1989;2:358-367.

16. Mohan JC, Sethi KK, Arora R, Khalilullah M. Cross sectional echocardiographic left ventricular ejection fraction: method based variability. *Indian Heart J*. 1992;44(1):23-28.

17. Alex L, Russo I, Holoborodko V, Frangogiannis NG. Characterization of a mouse model of obesity-related fibrotic cardiomyopathy that recapitulates features of human heart failure with preserved ejection fraction. *Am J Physiol Heart Circ Physiol*. 2018;315(4):H934-H949. doi:10.1152/ajpheart.00238.2018

18. Horgan S, Watson C, Glezeva N, Baugh J. Murine models of diastolic dysfunction and heart failure with preserved ejection fraction. *Journal of cardiac failure*. 2014;20(12):984-995. doi:10.1016/j.cardfail.2014.09.001 S1071-9164(14)01196-8 [pii]

19. Mohammed SF, Hussain S, Mirzoyev SA, Edwards WD, Maleszewski JJ, Redfield MM. Coronary microvascular rarefaction and myocardial fibrosis in heart failure with preserved ejection fraction. *Circulation*. 2015;131(6):550-559. doi:CIRCULATIONAHA.114.009625 [pii] 10.1161/CIRCULATIONAHA.114.009625

20. Kritikou E, Kuiper J, Kovanen PT, Bot I. The impact of mast cells on cardiovascular diseases. *Eur J Pharmacol*. 2016;778:103-115. doi:10.1016/j.ejphar.2015.04.050

21. Mikelis CM, Simaan M, Ando K, Fukuhara S, Sakurai A, Amornphimoltham P, Masedunskas A, Weigert R, Chavakis T, Adams RH, Offermanns S, Mochizuki N, Zheng Y, Gutkind JS. RhoA and ROCK mediate histamine-induced vascular leakage and anaphylactic shock. *Nat Commun*. 2015;6:6725. doi:10.1038/ncomms7725

22. Elieh Ali Komi D, Wöhrl S, Bielory L. Mast Cell Biology at Molecular Level: a Comprehensive Review. *Clin Rev Allergy Immunol*. Published online December 12, 2019. doi:10.1007/s12016-019-08769-2

23. Pant T, Dhanasekaran A, Bai X, Zhao M, Thorp EB, Forbess JM, Bosnjak ZJ, Ge Z-D. Genome-wide differential expression profiling of lncRNAs and mRNAs associated with early diabetic cardiomyopathy. *Sci Rep*. 2019;9(1):15345. doi:10.1038/s41598-019-51872-9

24. Hanif W, Alex L, Su Y, Shinde AV, Russo I, Li N, Frangogiannis NG. Left atrial remodeling, hypertrophy, and fibrosis in mouse models of heart failure. *Cardiovasc Pathol*. 2017;30:27-37. doi:S1054-8807(17)30050-9 [pii] 10.1016/j.carpath.2017.06.003

25. Alex L, Russo I, Holoborodko V, Frangogiannis NG. Characterization of a mouse model of obesity-related fibrotic cardiomyopathy that recapitulates features of human heart failure with preserved ejection fraction. *Am J Physiol Heart Circ Physiol*. 2018;315(4):H934-H949. doi:10.1152/ajpheart.00238.2018

26. Tromp J, Westenbrink BD, Ouwerkerk W, van Veldhuisen DJ, Samani NJ, Ponikowski P, Metra M, Anker SD, Cleland JG, Dickstein K, Filippatos G, van der Harst P, Lang CC, Ng LL, Zannad F, Zwinderman AH, Hillege HL, van der Meer P, Voors AA. Identifying Pathophysiological Mechanisms in Heart Failure With Reduced Versus Preserved Ejection Fraction. *J Am Coll Cardiol*. 2018;72(10):1081-1090. doi:10.1016/j.jacc.2018.06.050

27. Shah AM, Pfeffer MA. The many faces of heart failure with preserved ejection fraction. *Nature Reviews Cardiology*. 2012;9(10):555-556. doi:10.1038/nrcardio.2012.123

28. Schirone L, Forte M, Palmerio S, Yee D, Nocella C, Angelini F, Pagano F, Schiavon S, Bordin A, Carrizzo A, Vecchione C, Valenti V, Chimenti I, De Falco E, Sciarretta S, Frati G. A Review of the Molecular Mechanisms Underlying the Development and Progression of Cardiac Remodeling. *Oxid Med Cell Longev*. 2017;2017:3920195. doi:10.1155/2017/3920195

29. Hermans M, Lennep JR van, van Daele P, Bot I. Mast Cells in Cardiovascular Disease: From Bench to Bedside. *Int J Mol Sci*. 2019;20(14). doi:10.3390/ijms20143395

30. Mohajeri M, Kovanen PT, Bianconi V, Pirro M, Cicero AFG, Sahebkar A. Mast cell tryptase - Marker and maker of cardiovascular diseases. *Pharmacol Ther*. 2019;199:91-110. doi:10.1016/j.pharmthera.2019.03.008

31. Wang H, da Silva J, Alencar A, Zapata-Sudo G, Lin MR, Sun X, Ahmad S, Ferrario CM, Groban L. Mast Cell Inhibition Attenuates Cardiac Remodeling and Diastolic Dysfunction in Middle-aged, Ovariectomized Fischer 344 × Brown Norway Rats. *J Cardiovasc Pharmacol*. 2016;68(1):49-57. doi:10.1097/FJC.0000000000000385

32. Huang ZG, Jin Q, Fan M, Cong XL, Han SF, Gao H, Shan Y. Myocardial remodeling in diabetic cardiomyopathy associated with cardiac mast cell activation. *PLoS ONE*. 2013;8(3):e60827. doi:10.1371/journal.pone.0060827

33. Kovanen PT, Mänttäri M, Palosuo T, Manninen V, Aho K. Prediction of myocardial infarction in dyslipidemic men by elevated levels of immunoglobulin classes A, E, and G, but not M. *Arch Intern Med*. 1998;158(13):1434-1439. doi:10.1001/archinte.158.13.1434

34. Korkmaz ME, Oto A, Saraçlar Y, Oram E, Oram A, Ugurlu S, Karamehmetoglu A, Karaagaoglu E. Levels of IgE in the serum of patients with coronary arterial disease. *Int J Cardiol*. 1991;31(2):199-204. doi:10.1016/0167-5273(91)90216-c

35. Xu Z, Wang T, Guo X, Li Y, Hu Y, Ma C, Wang J. The Relationship of Serum Antigen-Specific and Total Immunoglobulin E with Adult Cardiovascular Diseases. *Int J Med Sci*. 2018;15(11):1098-1104. doi:10.7150/ijms.25857

36. Liu H, Fu Y, Wang K. Asthma and risk of coronary heart disease: A meta-analysis of cohort studies. *Ann Allergy Asthma Immunol*. 2017;118(6):689-695. doi:10.1016/j.anai.2017.03.012

37. Unal D, Gelincik A, Elitok A, Demir S, Olgac M, Coskun R, Kocaaga M, Colakoglu B, Buyukozturk S. Impact of high serum Immunoglobulin E levels on the risk of atherosclerosis in humans. *Asia Pac Allergy*. 2017;7(2):74-81. doi:10.5415/apallergy.2017.7.2.74

38. Zhang J, Cai W-K, Zhang Z, Wang P, Lin X-Q, Feng J, Fu S-C, He G-H. Cardioprotective effect of histamine H2 antagonists in congestive heart failure: A systematic review and meta-analysis. *Medicine (Baltimore)*. 2018;97(15):e0409. doi:10.1097/MD.0000000000010409

39. Omae K, Ogawa T, Yoshikawa M, Nitta K. The use of H1-receptor antagonists and left ventricular remodeling in patients on chronic hemodialysis. *Heart Vessels*. 2010;25(2):163-169. doi:10.1007/s00380-009-1183-9

40. Matsumori A, Yamamoto K, Shimada M. Cetirizine a histamine H1 receptor antagonist improves viral myocarditis. *J Inflamm (Lond)*. 2010;7:39. doi:10.1186/1476-9255-7-39

Highlights

- $Lepr^{db/db}$ female display increased cardiac mast cell activation
- Cardiac mast cell activation participates in the development of cardiac small vessel disease, notably via Histamine release.
- Cardiac mast cell activation participate in the development of diastolic dysfunction
- Mast cell stabilizer or H1 receptor antagonist may be used to prevent the occurrence of diastolic dysfunction in the setting of type diabetes and obesity.

Figures and Figure Legends

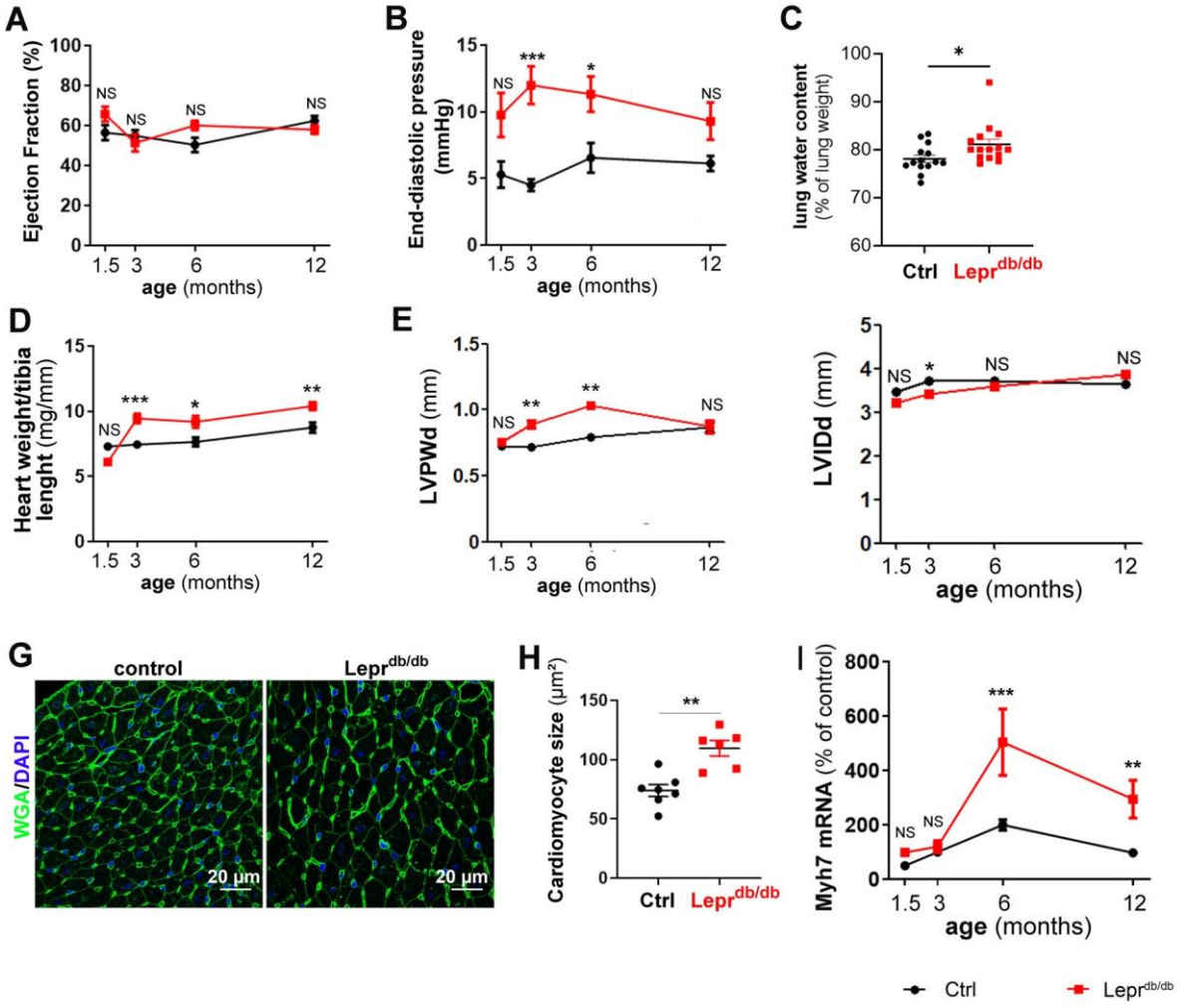

Figure 1: Lepr$^{db/db}$ female mice have diastolic dysfunction from 3 months of age. Lepr$^{db/db}$ female mice and their control Lepr^{db}/+ littermates were subjected to echocardiography, LV catheterization and sacrificed at the indicated time points (n=8 to 15 mice per group). (**A**) Ejection faction was measured via echocardiography. (**B**) End diastolic pressure was measured using a pressure catheter. (**C**) Pulmonary edema was quantified as the percentage of water of in lungs (water content in g over lung weight). (**D**) Heart hypertrophy was assessed by calculating the heart weight over tibia length ratio. (**E**) End diastolic left ventricular posterior wall thickness during (LVPWd) was measured via echocardiography. (**F**)

End diastolic left ventricular internal diameter was measured via echocardiography. (**G**) Heart cross sections from 3 month old mice were stained with FITC-labeled WGA. Representative pictures are shown (scale bar: 20 µm). (**H**) The mean cardiomyocyte surface area was measured. (**I**) Myh7 mRNA expression was measured via RT-qPCR in heart biopsies. *: p≤0.05; **: p≤0.01. ***: p≤0.001. NS: not significant. Two way ANOVA followed by Sidak's multiple comparison test or Mann Whitney test.

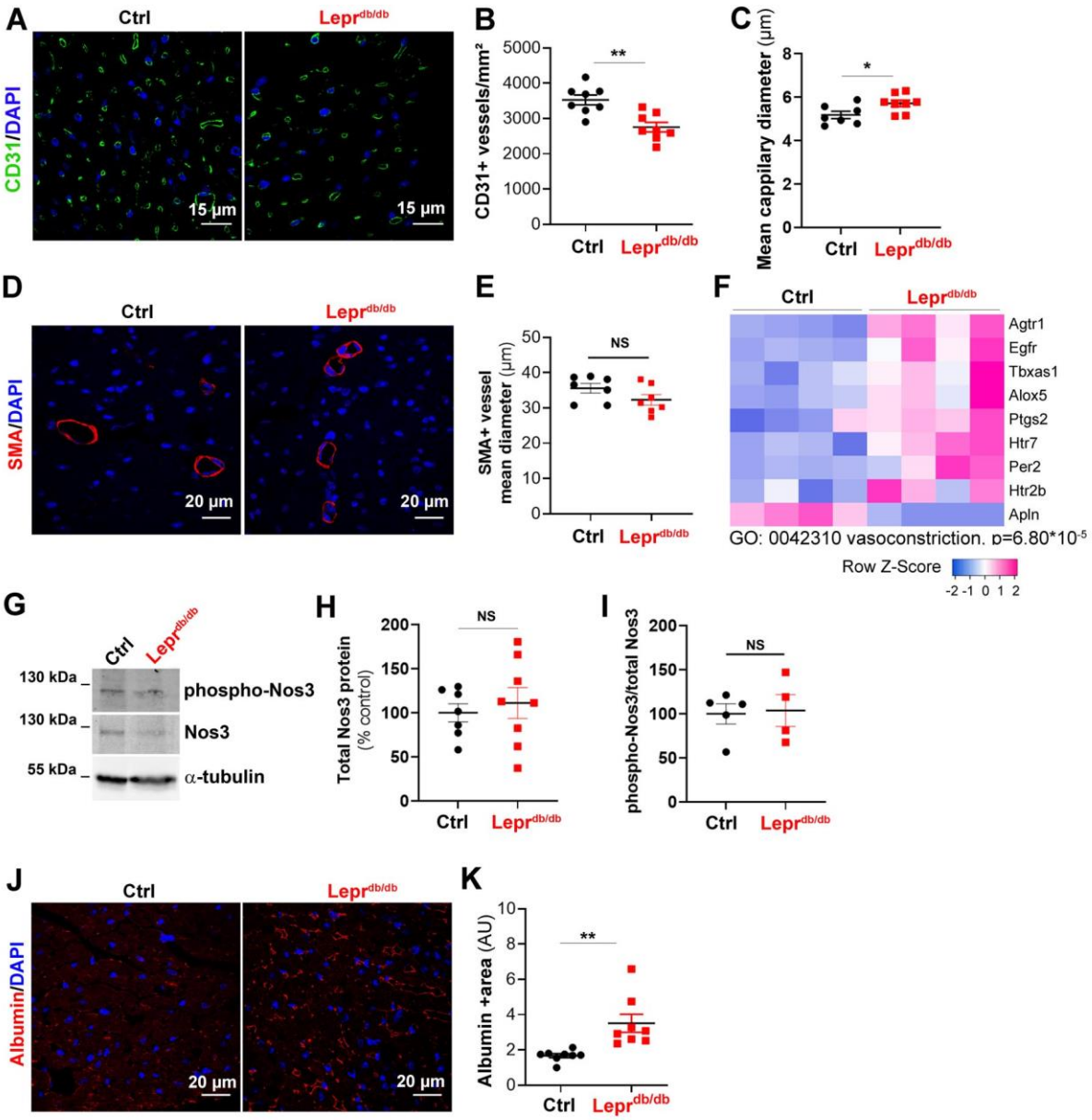

Figure 2: Lepr$^{db/db}$ female mice have cardiac microvascular dysfunction. Lepr$^{db/db}$ female mice and their control Lepr^{db}/+ littermates were sacrificed at 3 months of age. (**A**) Heart cross sections were immuno-stained with anti-CD31 antibodies to identify ECs. Representative pictures are shown (scale bar: 15 µm). (**B**) Capillary density was quantified as the number of CD31+ vessels/mm² (n 8 mice/ group). (**C**) The mean cardiac capillary diameter was measured (n=8 and 7 mice/ group). (**D**) Heart cross sections were immuno-stained with anti-SMA antibodies to identify smooth muscle cells. Representative pictures are shown (scale bar: 20 µm). (**E**) The mean cardiac arteriole diameter was measured (n=7

mice/ group). (**F**) RNA sequencing analysis of the cardiac vascular fraction revealed that "vasoconstriction" is one of the biological processes significantly increased in $Lepr^{db/db}$ mice (n=4 mice/group). (**G**) Phosphorylated-Nos3 (S1177) and total Nos3 protein levels were assessed via western blot analyses in total heart biopsies and (**H, I**) quantified using Image J software (n=8 and 7 mice/group). (**J**) Heart cross sections were immuno-stained with anti-Albumin antibodies to assess vascular leakage. Representative pictures are shown (scale bar: 20 µm). (**K**) Albumin extravasation was measured as the albumin+ surface area. ² (n=6 and 15 mice/ group). *: p≤0.05, **: p≤0.01, NS: not significant. Mann Whitney test.

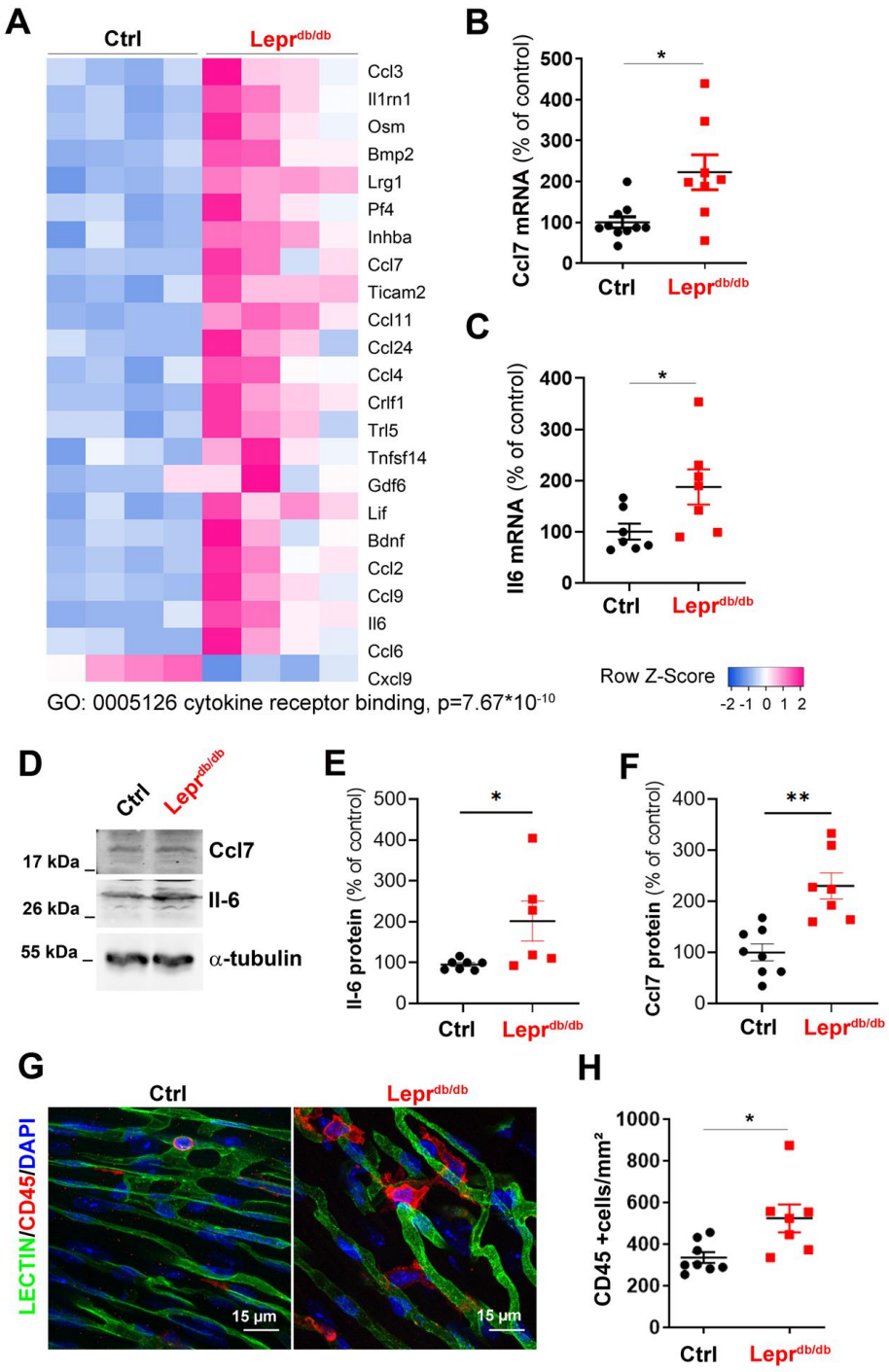

Figure 3: Lepr$^{db/db}$ female mice have increased cardiac inflammation. Lepr$^{db/db}$ female mice and their control Lepr^{db}/+ littermates were sacrificed at 3 months of age. (**A**) RNA sequencing analysis of the cardiac vascular fraction revealed that "Cytokine receptor binding" is one of the molecular function significantly increased in Lepr$^{db/db}$ mice (n=4 mice/group). Ccl7 (**B**) and Il-6 (**C**) mRNA expression was measured via RT-qPCR in total heart

biopsies (n=10 mice/group). (**D**) Ccl7 and Il-6 protein level were assessed by western blot analysis (**E, F**) and quantified using Image J software. (**G**) BS1-lectin-FITC-perfused heart cross sections were immuno-stained with anti-CD45 antibodies to assess cardiac inflammation. Representative pictures are shown (scale bar: 15 µm). (**H**) Leucocyte infiltration was measured as the number of CD45+ cells/mm² (n=7 and 8 mice/ group). *: p≤0.05; **: p≤0.01. Mann Whitney test.

A

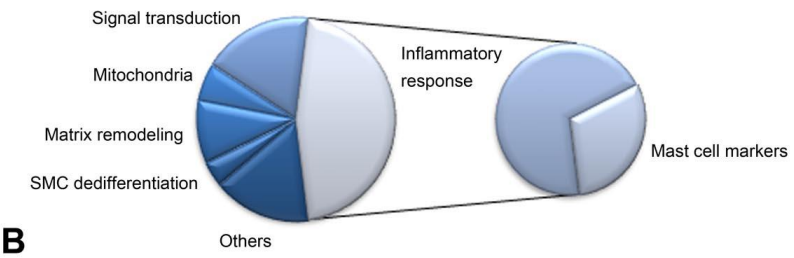

B

gene ID	full name	logFC	Fold change	p value	FDR
Tpsab1	Tryptase alpha/beta-1	3.0139	**8.07**	2.97E-13	2.14E-11
Fcer1a	High affinity immunoglobulin epsilon receptor subunit alpha	2.6082	**6.10**	1.31E-5	1.52E-04
Mcpt2	Mast cell protease 2	2.4391	**5.42**	1.84E-22	7.67E-20
Tpsb2	Tryptase beta-2	2.3514	**5.10**	1.43E-11	7.66E-10
Cma1	Cma1 chymase 1. mast cell	2.2210	**4.66**	6.23E-13	4.13E-11
Cpa3	Carboxypeptidase A3. mast cell	2.2109	**4.63**	2.95E-13	2.13E-11
Mcpt4	Mast cell protease 4	2.1600	**4.47**	2.93E-10	1.16E-08

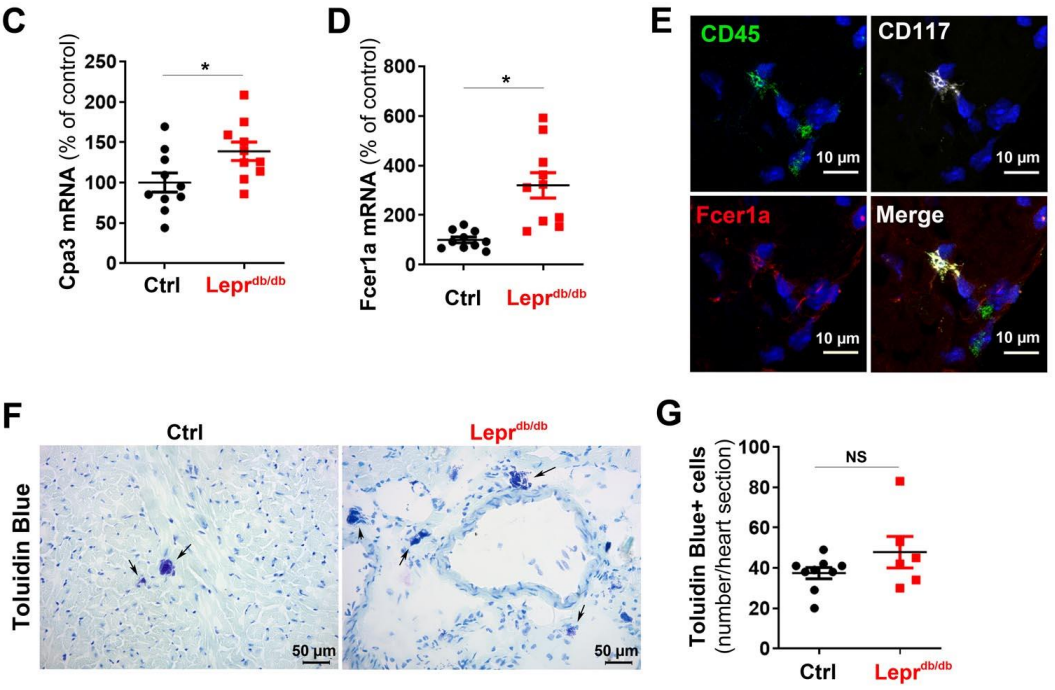

Figure 4: Lepr$^{db/db}$ female mice have increased cardiac inflammation. Lepr$^{db/db}$ female mice and their control Lepr^{db}/+ littermates were sacrificed at 3 months of age. (**A**) RNA sequencing analysis of the cardiac vascular fraction was performed. Among the 50 most upregulated gene in Lepr$^{db/db}$ female mice, 7 are mast cell markers. (**B**) List of mast cell marker upregulated in Lepr$^{db/db}$ female mice. Cpa3 (**C**) and Fcer1a (**D**) mRNA expression was measured via RT-qPCR in total heart biopsies (n=10 mice/group). (**E**) Heart cross sections were co-immunostained with anti-CD45 (in green), anti-CD117 (in white) and anti-Fcer1a (in

red) antibodies (scale bar: 10 µm). (**F**) Heart cross sections were stained with Toluidine Blue to identify mast cells. Representative pictures are shown (scale bar: 50 µm). (**G**) Mast cell infiltration was quantified as the number of toluidine blue+ cells/heart section. *: $p \leq 0.05$; NS: not significant. Mann Whitney test.

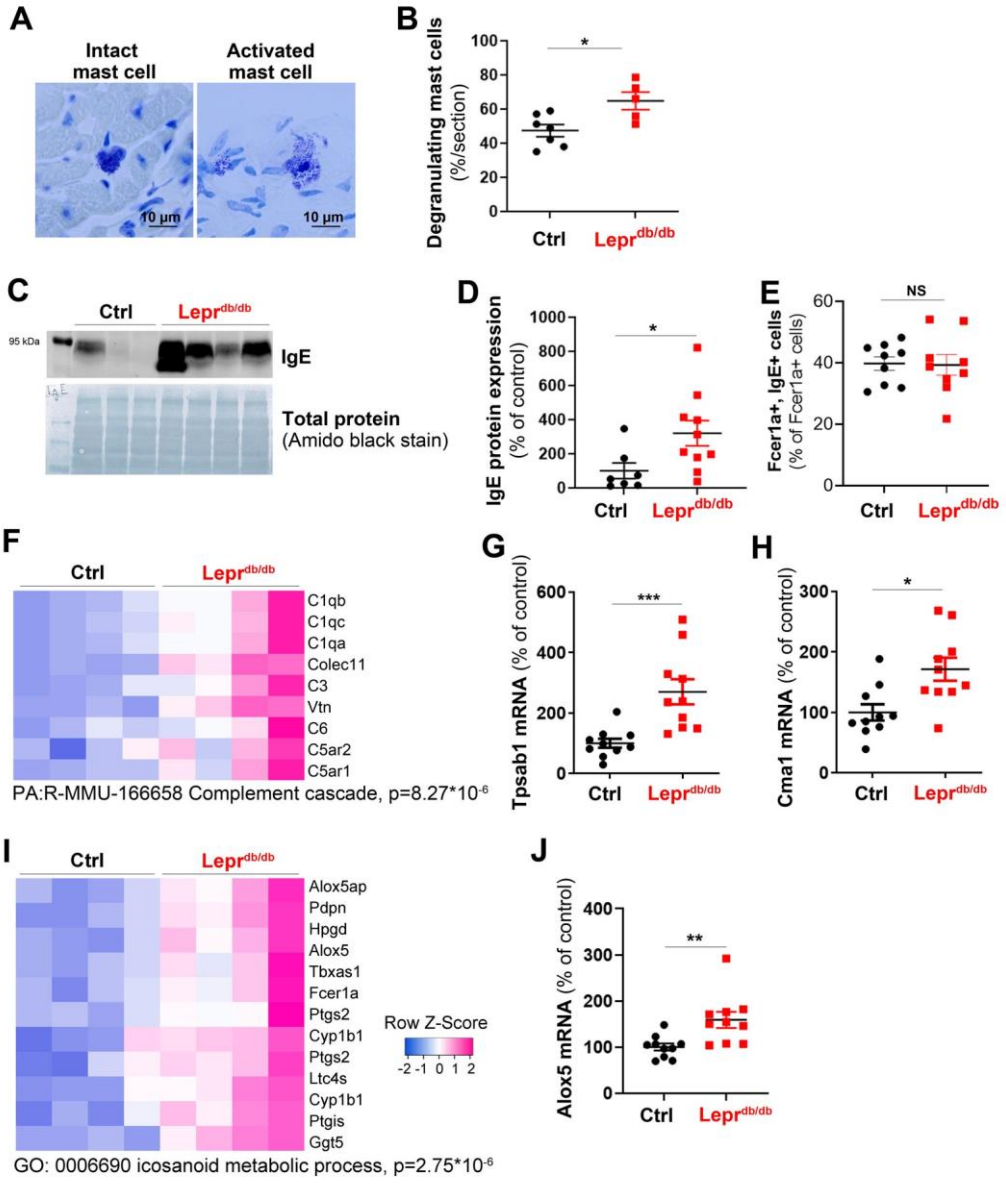

Figure 5: Lepr$^{db/db}$ female mice have increased cardiac mast cell activation. Lepr$^{db/db}$ female mice and their control Lepr^{db}/+ littermates were sacrificed at 3 months of age. (**A**) Heart cross sections were stained with Toluidine Blue to identify mast cells degranulation (scale bar: 10 µm). (**B**) The percentage of degranulating mast cell was quantified. (**C**) Plasmatic IgE level was assessed by western blot analysis and (**D**) quantified (n=10 and 7 mice/group). (**E**) CD45+ positive cells were isolated from total heart biopsies, Fcer1a, IgE double positive cells were counted via flow cytometry analysis (n=9 mice/group). (**F**) RNA sequencing analysis of the cardiac vascular fraction revealed that "Complement cascade" is one of the reactome

pathway significantly increased in Lepr$^{db/db}$ mice (n=4 mice/group). Tpsab1 (**G**) and Cma1 (**H**) mRNA expression was measured via RT-qPCR in total heart biopsies (n=10 mice/group). (**I**) RNA sequencing analysis of the cardiac vascular fraction revealed that "Icosanoid metabolic process" is one of the molecular function significantly increased in Lepr$^{db/db}$ mice (n=4 mice/group). (**J**) Alox5 mRNA expression was measured via RT-qPCR in total heart biopsies (n=10 mice/group). *: p≤0.05; **: p≤0.01; ***: p≤0.001. Mann Whitney test.

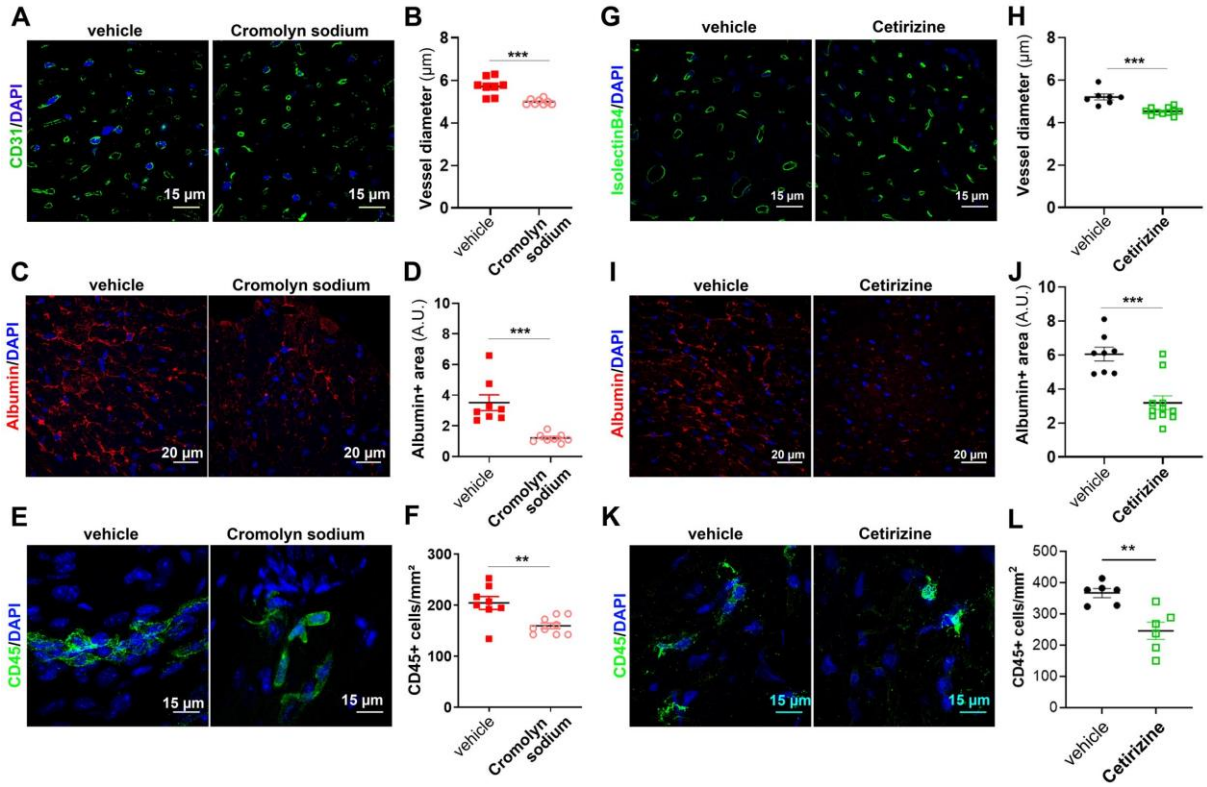

Figure 6: Mast cells promote cardiac small vessel disease in Lepr$^{db/db}$ female mice. (**A-F**) 2 month old Lepr$^{db/db}$ female mice were treated or not with 50 mg/kg/day cromolyn sodium for 28 days. Mice were sacrificed at 3 months of age. (**A**) Heart cross sections were immune-stained with anti-CD31 antibodies to identify ECs. Representative pictures are shown (scale bar: 15 µm). (**B**) The mean cardiac capillary diameter was measured (n= 8 mice/ group). (**C**) Heart cross sections were immunostained with anti-albumin antibodies to assess vascular leakage. Representative pictures are shown (scale bar: 20 µm). (**D**) Albumin extravasation was measured as the albumin+ surface area (n=8 mice/ group). (**E**) Heart cross sections were immunostained with anti-CD45 antibodies to assess cardiac inflammation. Representative pictures are shown (scale bar: 15 µm). (**F**) Leucocyte infiltration was measured as the number of CD45+ cells/mm² (n=10 mice/ group). (**G-H**) 2 month old Lepr$^{db/db}$ female mice were treated or not with 4 mg/kg/day cetirizine for 28 days. Mice were sacrificed at 3 months of age. (**G**) Heart cross sections were stained with FITC-labelled Isolectin B4 identify

ECs. Representative pictures are shown (scale bar: 15 µm). (**H**) The mean cardiac capillary diameter was measured (n= 10 and 7 mice/ group respectively). (**I**) Heart cross sections were immunostained with anti-albumin antibodies to assess vascular leakage. Representative pictures are shown (scale bar: 20 µm). (**J**) Albumin extravasation was measured as the albumin+ surface area (n= 10 and 7 mice/ group respectively). (**K**) Heart cross sections were immunostained with anti-CD45 antibodies to assess cardiac inflammation. Representative pictures are shown (scale bar: 15 µm). (**L**) Leucocyte infiltration was measured as the number of CD45+ cells/mm² (n=10 mice/group). **: p≤0.01; ***: p≤0.001. Mann Whitney test.

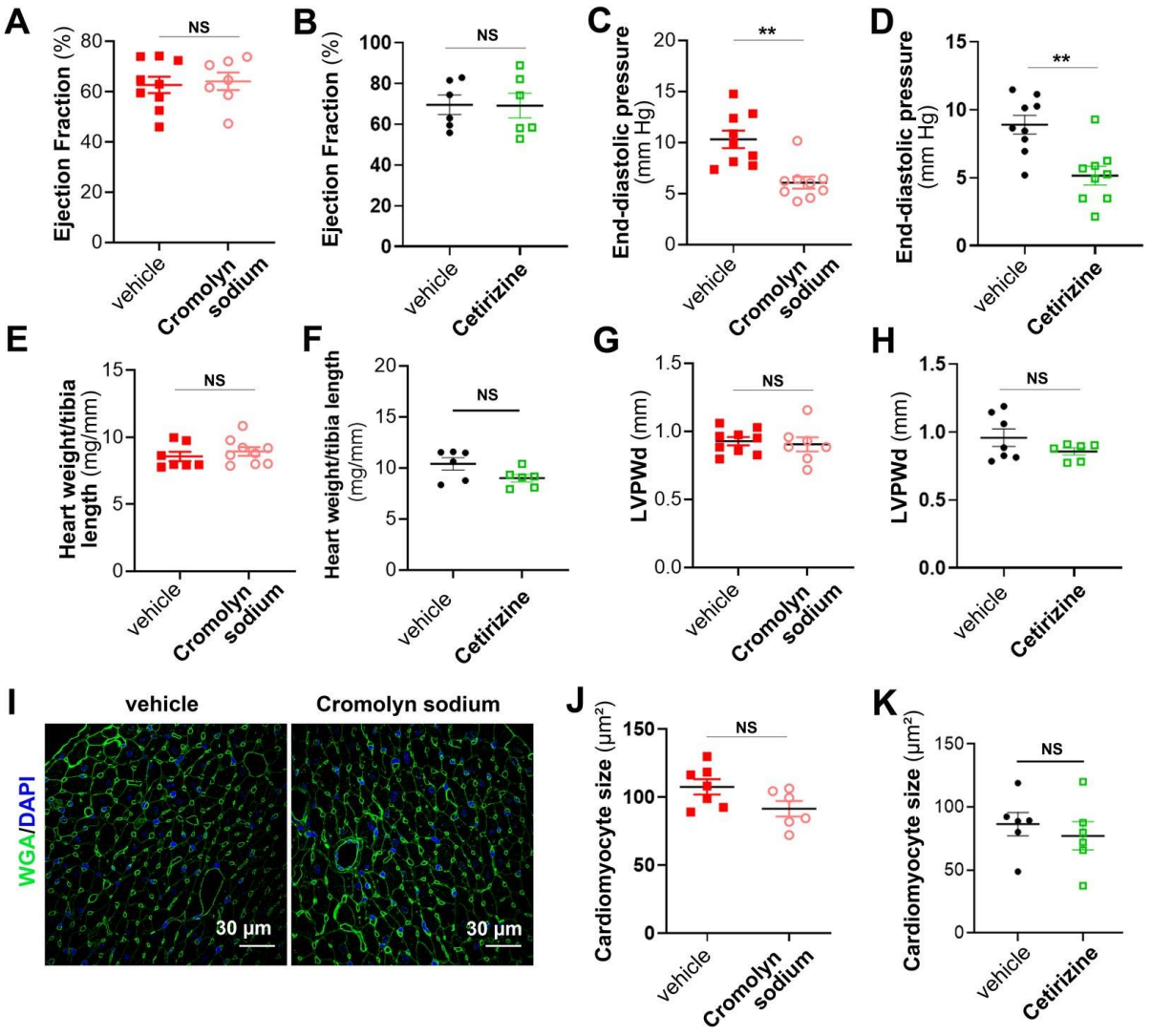

Figure 7: Mast cells promote diastolic dysfunction in Lepr$^{db/db}$ female mice. 2 month old Lepr$^{db/db}$ female mice were either treated with 50 mg/kg/day cromolyn sodium vs control vehicle or 4 mg/kg/day cetirizine vs control vehicle for 28 days. At 3 months of age, mice were subjected to echocardiography, LV catheterization and sacrificed. (**A-B**) Ejection faction was measured via echocardiography (n=6-9 mice/group). (**C-D**) End diastolic pressure was measured using a pressure catheter (n=9 mice/group). (**E-F**) Heart hypertrophy was assessed by calculating the heart weight over tibia length ratio (n=9 mice/group). (**G-H**) Left ventricular posterior wall thickness during diastole (LVPWd) was measured via echocardiography (n=6-9 mice/group). (**I**) Heart cross sections were stained with FITC-

labeled WGA. Representative pictures are shown (scale bar: 30 µm). (**J-K**) The mean cardiomyocyte surface area was measured. **: p≤0.01; NS: not significant. Mann Whitney test.